


Article

Quantum Photonic Simulation of Spin-Magnetic Field Coupling and Atom-Optical Field Interaction

Jesús Liñares ^{*,†} , Xesús Prieto-Blanco [†], Gabriel M. Carral [†] and María C. Nistal [†]

Quantum Materials and Photonics Research Group, Optics Area, Department of Applied Physics, Faculty of Physics/Faculty of Optics and Optometry, Campus Vida s/n, University of Santiago de Compostela, E-15782 Santiago de Compostela, Galicia, Spain; xesus.prieto.blanco@usc.es (X.P.-B.); gabrielmaria.carral@rai.usc.es (G.M.C.); mconcepcion.nistal@usc.es (M.C.N.)

* Correspondence: suso.linares.beiras@usc.es

† These authors contributed equally to this work.

Received: 8 November 2020; Accepted: 7 December 2020; Published: 10 December 2020



Abstract: In this work, we present the physical simulation of the dynamical and topological properties of atom-field quantum interacting systems by means of integrated quantum photonic devices. In particular, we simulate mechanical systems used, for example, for quantum processing and requiring a very complex technology such as a spin-1/2 particle interacting with an external classical time-dependent magnetic field and a two-level atom under the action of an external classical time-dependent electric (optical) field (light-matter interaction). The photonic device consists of integrated optical waveguides supporting two collinear or codirectional modes, which are coupled by integrated optical gratings. We show that the single-photon quantum description of the dynamics of this photonic device is a quantum physical simulation of both aforementioned interacting systems. The two-mode photonic device with a single-photon quantum state represents the quantum system, and the optical grating corresponds to an external field. Likewise, we also present the generation of Aharonov–Anandan geometric phases within this photonic device, which also appear in the simulated systems. On the other hand, this photonic simulator can be regarded as a basic brick for constructing more complex photonic simulators. We present a few examples where optical gratings interacting with several collinear and/or codirectional modes are used in order to illustrate the new possibilities for quantum simulation.

Keywords: integrated photonics; quantum optics; quantum simulation

1. Introduction

One of the most promising tasks in quantum science and technology is the implementation of quantum simulations. Its physical foundation is based on the fact that the dynamics of a quantum system is governed by its Hamiltonian \hat{H} (time evolution) or momentum operator \hat{M} (spatial evolution), that is given a Hilbert space \mathcal{H} and some input state $|\Psi(0)\rangle \in \mathcal{H}$, the full evolution of the system is given by the action of the evolution operator on such a state. The evolution operator can be either the time evolution one $\hat{U}_t = \exp(-i\hat{H}t/\hbar)$, which comes from the Schrödinger equation $-i\hbar\partial|\Psi\rangle/\partial t = \hat{H}|\Psi\rangle$, that is $|\Psi(t)\rangle = \hat{U}_t|\Psi(0)\rangle$, or its spatial counterpart $\hat{U}_s = \exp(i\hat{M}s/\hbar)$, which comes from the momentum operator in the position representation, that is $i\hbar\partial|\Psi\rangle/\partial s = \hat{M}|\Psi\rangle$, where s is the spatial variable that defines the direction along which the system evolves (it can be, for instance, the z -direction) then $|\Psi(s)\rangle = \hat{U}_s|\Psi(0)\rangle$. One is perhaps more familiar with the temporal case $|\Psi(t)\rangle = \hat{U}_t|\Psi(0)\rangle$, but note that the spatial case is totally analogous [1,2]. Now, as it occurs in nature that very different and unrelated quantum systems share analogous Hamiltonians or momentum operators, the dynamics of these systems will be analogous. This implies that if we have some system of interest, we will be able

to mimic its behavior (evolution) by means of other very different system. This last system, which is required to be fully controllable by the experimenter, constitutes a quantum simulator [3,4] of the system of interest.

On the other hand, the importance of making quantum simulations obeys various reasons. First of all, whether classical or quantum, simulation is often an indispensable tool in science. Physical systems can be very complicated to study. If we find a way to mimic their behavior in a manageable way, their dynamics can be analyzed with much less difficulty, much less expensively, and much faster [3]. For instance, we can imagine that the system of interest is one whose working conditions are fragile and very sensitive to small perturbations. It could also be that those conditions are very specific and/or hard (even impossible) to achieve in the laboratory. Simulating these complicated systems will, in principle, improve our knowledge about them with much ease. Secondly, quantum simulation offers a crucial advantage over classical simulation. Quantum systems have a greater information storing capacity than classical systems; thus, a quantum simulator, which is a quantum system itself, will require much fewer physical resources than a classical simulator to store the same amount of information. Furthermore, classical simulations find difficulties simulating quantum systems when strong entanglement is present [3]. Finally, it is possible that the potential applications of a quantum system may be better implemented using a quantum simulation [5], if it happens that the quantum simulation parameters are easier to handle, compared to those of the quantum system of interest, in the sense of greater tunability [4]. All of this strongly suggests the need for quantum simulations. Formally, one has a quantum device, called the quantum simulator, which reproduces the evolution of the system of interest, the quantum system. Following [4], let us call the initial input state of the quantum system $|\phi(0)\rangle$, which evolves to $|\phi(\zeta)\rangle$, where ζ stands either for time or some spatial coordinate, under the evolution operator $\hat{U} = \exp(i\hat{O}\zeta/\hbar)$. Here, \hat{O} can be a Hamiltonian ($-\hat{H}$) or a momentum operator (\hat{M}). The quantum simulator, on the other hand, starts in the state $|\psi(0)\rangle$ and evolves to $|\psi(\zeta)\rangle$ under the action of the operator $\hat{U}' = \exp(i\hat{O}'\zeta/\hbar)$. Since we have a system and a simulator, there exists a correspondence relating these elements, that is a correspondence between $|\phi(0)\rangle \leftrightarrow |\psi(0)\rangle$, $|\phi(\zeta)\rangle \leftrightarrow |\psi(\zeta)\rangle$, $\hat{U} \leftrightarrow \hat{U}'$, and thus, $\hat{O} \leftrightarrow \hat{O}'$. This is revealed via measurements on both systems. The greater the accuracy of this correspondence, the more one can trust the simulator [3].

In this work, we present an integrated quantum photonic simulator for atom-field quantum interacting systems. It is based on optical gratings and can be regarded as a basic brick for constructing more complex photonic simulators. First of all, we would like to stress the high interest in quantum photonic simulators; for instance, integrated photonic structures allow simulating a number of condensed matter effects such as Anderson localization, Mott transition, etc. [6], and more recently, anyonic interaction has been simulated by using an array of channel optical waveguides with a helically bent axis [7]. In our case, we will simulate in an integrated photonic device the dynamical and topological properties of two very well-known quantum interacting systems. This is relevant since a way to check the fidelity of a simulation is testing the same physical model of the dynamics with different systems and then comparing the results [5]. The two systems to be simulated are the well-known interaction of a spin-1/2 particle under a time-dependent external classical magnetic field (see for instance [8]) and the interaction of a two-level atom with an external classical electric field (see for instance [9]) which are used, at present, for implementing quantum information devices for quantum processing, quantum computation, and so on [8]. It is also well known that these mechanical systems require a very complex technology. We will take a standard photonic device, that is a two-mode planar guide modulated by an integrated grating (see for instance [10]) in which a single-photon quantum state is propagated. We will show that it can emulate both the dynamical and geometrical properties of the two aforementioned systems. As mentioned, this photonic simulator based on integrated optical gratings can be regarded as a basic brick for more complex photonic simulators; thus, the results obtained can be extended to multi-level systems or to several concatenated two-mode systems simulating concatenated temporal operations. Addressing practical issues, this simulator will also benefit from some advantages of classical and quantum integrated photonics [6,11,12], such as

the fast and energetically efficient operation and miniaturization capabilities of integrated photonics, which favor scalability. Moreover, integrated photonic devices are becoming some of the most powerful and appealing technologies for classical and quantum information [13,14]. Finally, we must stress that although we present a photonic device for quantum simulation, it can be also used to implement quantum operations and/or effects with the photonic device itself such as logic gates, geometric phases, and so on.

The plan of the paper is as follows: In Section 2, we briefly present the Hamiltonian of the quantum interacting systems, in a suitable form for their photonic simulation, along with the physical parameters and some useful solutions. In Section 3, starting from quantum states as single-photon states, an integrated photonic device for the quantum simulation of both a spin-magnetic field coupling and light-matter interaction is presented, along with the limits of this simulation. In Section 4, quantum simulation of geometric phases is studied. Finally, a summary is presented in Section 5.

2. Mechanical Interacting Systems

In this section, we present the main results about the mechanical interacting systems whose dynamic and topological properties are going to be simulated with an integrated photonic device. The primary aim is to write the Hamiltonians of these systems in a suitable form to facilitate the study of their photonic simulations.

2.1. Spin-1/2 Particle Interacting with a Magnetic Field

The Hamiltonian of a spin particle interacting with a magnetic field is given by $\hat{H} = -\boldsymbol{\mu} \cdot \mathbf{B}$, where $\boldsymbol{\mu}$ is the magnetic moment of the particle, which is proportional to the spin operator, and \mathbf{B} is the magnetic field. Let us consider a spin- $\frac{1}{2}$ particle, then $\boldsymbol{\mu} = \frac{1}{2}\mu\boldsymbol{\sigma}$, where $\mu = \hbar\gamma_p$, with γ_p the gyromagnetic ratio of the particle ($p = e$ for an electron, $p = n$ for a neutron, etc.), and $\boldsymbol{\sigma} = (\sigma_x, \sigma_y, \sigma_z)$ are the Pauli matrices. Moreover, we choose a time-dependent magnetic field, which, by assuming a sinusoidal dependence in time with frequency ω , is written as $\mathbf{B} = B_0(\sin\theta \cos\omega t, -\sin\theta \sin\omega t, \cos\theta)$, representing a magnetic field of modulus B_0 rotated an angle θ with respect to the z-axis and spinning around this same axis with a frequency ω . We can then write the well-known spin-magnetic Hamiltonian as (see for instance [8]):

$$\hat{H}(t) = -\frac{\hbar}{2}\gamma_p B_0 \cos\theta \sigma_z - \frac{\hbar}{2}\gamma_p B_0 \sin\theta (\cos\omega t \sigma_x - \sin\omega t \sigma_y). \tag{1}$$

By taking into account the expressions of the Pauli matrices, then the above Hamiltonian gives rise to the following time-dependent Schrödinger equation:

$$i\hbar \frac{\partial}{\partial t} |\Psi(t)\rangle = -\frac{\hbar}{2}\gamma_p B_0 \begin{pmatrix} \cos\theta & \sin\theta \exp(i\omega t) \\ \sin\theta \exp(-i\omega t) & -\cos\theta \end{pmatrix} |\Psi(t)\rangle = \equiv \hat{H}(t) |\Psi(t)\rangle. \tag{2}$$

This time-dependent Hamiltonian is enough for our simulation purposes. Note that for the neutron case, we have the well-known Nuclear Magnetic Resonance (NMR). The solution of the equation above can be obtained as a time-dependent linear combination of down and up spin states, $|0\rangle$ and $|1\rangle$, of the particle, that is $|\Psi(t)\rangle = c_0(t)|0\rangle + c_1(t)|1\rangle$. Thus, by using the vector representation of $|\Psi(t)\rangle$ and the matrix Hamiltonian given by Equation (2), the Schrödinger equation can be rewritten as follows:

$$i\hbar \frac{dc_n(t)}{dt} = E_n \cos\theta c_n(t) + i \sum_{n \neq m} C_{nm}(t) c_m(t). \tag{3}$$

with $n = 0, 1$, $E_0 = -\frac{\hbar\gamma_p}{2}B_0$ and $E_1 = \frac{\hbar\gamma_p}{2}B_0$ the eigenvalues of spin states when a static magnetic field along z-direction is applied, and $C_{01}(t) = C_{10}^*(t) = -\frac{\hbar\gamma_p}{2}B_0 \sin \theta \exp(i\omega t)$ the coupling coefficients. On the other hand, it is interesting, for the sake of expositional convenience, to present the main results about the dynamics of the system. First of all, in order to simplify things, we can shift to a reference frame that is rotating at a frequency ω by means of the following unitary transformation:

$$|\eta(t)\rangle = \hat{U}(t, \omega)|\Psi(t)\rangle = \exp(-i\omega\sigma_z t/2)|\Psi(t)\rangle; \tag{4}$$

therefore, by inserting $|\Psi(t)\rangle = \exp(i\omega\sigma_z t/2)|\eta(t)\rangle$ into the Schrödinger equation, we obtain, after some simple calculations, the following Hamiltonian acting on $|\eta(t)\rangle$:

$$\hat{H}'|\eta(t)\rangle = \frac{\hbar}{2} \begin{pmatrix} -\gamma_p B_0 \cos \theta + \omega & -\gamma_p B_0 \sin \theta \\ -\gamma_p B_0 \sin \theta & \gamma_p B_0 \cos \theta - \omega \end{pmatrix} |\eta(t)\rangle. \tag{5}$$

This Hamiltonian \hat{H}' can be rewritten as a product of the form $-\frac{\hbar}{2}\gamma_p(\sigma \cdot \mathbf{B}_{ef})$, with \mathbf{B}_{ef} an effective static magnetic field, that is,

$$\hat{H}' = -\frac{\hbar}{2}\gamma_p(\sigma \cdot \mathbf{B}_{ef}) = -\frac{\hbar}{2}\gamma_p B_0 \Delta \cos \theta' \sigma_z - \frac{\hbar}{2}\gamma_p B_0 \Delta \sin \theta' \sigma_x = -\frac{\hbar}{2}\Delta_o \begin{pmatrix} \cos \theta' & \sin \theta' \\ \sin \theta' & -\cos \theta' \end{pmatrix}, \tag{6}$$

with:

$$\Delta_o = \gamma_p B_0 \Delta = \gamma_p B'_o \tag{7}$$

and:

$$\Delta = \gamma_p B_0 \sqrt{1 - \frac{2\omega}{\gamma_p B_0} \cos \theta + \frac{\omega^2}{\gamma_p^2 B_0^2}}; \tag{8}$$

therefore, the effective magnetic field is given by $\mathbf{B}_{ef} = (B'_o \sin \theta', 0, B'_o \cos \theta')$, where B'_o and θ' are related to B_0 and θ by $B'_o = B_0 \Delta$, with $\sin \theta' = \gamma_p B_0 \sin \theta / \Delta_o = \sin \theta / \Delta$ and $\cos \theta' = \gamma_p B_0 [\cos \theta - (\omega / \gamma_p B_0)] / \Delta_o = [\cos \theta - (\omega / \gamma_p B_0)] / \Delta$. As seen from the expression for Δ , it would seem that for this reparametrization to have physical meaning, restrictions on the parameters would appear, as Δ contains a possible non-positive term under the square root. The worst case would be likely to happen if $\cos \theta = 1$, but one can find that the resulting quantity $1 - (2\hbar\omega / \mu B_0) + (\hbar\omega / \mu B_0)^2$ is never negative, for any value of the parameters.

Next, it is interesting to compute the eigenstates $|\eta\rangle$ and eigenvalues E_η of Hamiltonian \hat{H}' given by Equation (6), that is $|\eta(t)\rangle = \exp(-\frac{i}{\hbar}E_\eta t)|\eta(0)\rangle$. After a standard calculation, we have:

$$|\eta_+(0)\rangle = \cos \frac{\theta'}{2}|0\rangle + \sin \frac{\theta'}{2}|1\rangle, \quad |\eta_-(0)\rangle = \sin \frac{\theta'}{2}|0\rangle - \cos \frac{\theta'}{2}|1\rangle, \tag{9}$$

where $|0\rangle \equiv (1, 0)^T$ and $|1\rangle \equiv (0, 1)^T$, with T denoting the transpose. The eigenvalues are $E_\pm = \pm \frac{\hbar}{2}\Delta_o$, that is $E_\pm = \pm \frac{\hbar}{2}\gamma_p B'_o = \pm \frac{\hbar}{2}B'_o$. Therefore, by taking into account Equation (4), the full evolved states $|\Psi(t)\rangle$ can be easily obtained.

2.2. Two-Level Atom Interacting with an Electric (Optical) Field

On the other hand, let us consider a two-level atom coupled to a harmonic external classical electric field, which describes semiclassical light-matter interaction. As is usually done [9], we label the atomic levels as $|g\rangle$ (ground) and $|e\rangle$ (excited). They have energies $\hbar\omega_g$ and $\hbar\omega_e$, respectively.

Their energy difference is given by $\hbar\omega_0 = \hbar(\omega_e - \omega_g)$. The expression for this non-interacting part of the Hamiltonian can be formally written as follows:

$$\hat{H}_0 = \hbar\omega_g|g\rangle\langle g| + \hbar\omega_e|e\rangle\langle e| = \hbar\bar{\omega}\mathbf{I} + \hbar\omega_0\sigma_z/2, \tag{10}$$

where we used the matrix representation of $|g\rangle\langle g|$ and $|e\rangle\langle e|$, with $\bar{\omega} = (\omega_g + \omega_e)/2$, and \mathbf{I} the two-dimensional identity matrix. As for the interacting part, it is given by the dipole interaction (electric dipole approximation) between an external electric (optical) field and the atom. Indeed, by assuming, for the sake of simplicity, that the field is propagating along z , has a sinusoidal dependence in time with frequency ω , and is linearly polarized along the x -direction, then the electric (optical) field can be written as follows $\mathbf{E} = E_0 \cos(\omega(z/c - t)) \mathbf{u}_x$. Moreover, we disregard the spatial dependence of the electric (optical) field because the wavelength $\lambda = c/2\pi\omega$ is considered much larger than the atomic dimensions. Therefore, we apply the dipole or long-wavelength approximation, that is by assuming without loss of generality $\omega z/c = 2m\pi$, with m an integer, then $\mathbf{E} = E_0 \cos \omega t \mathbf{u}_x$, the electric-dipole interaction is given by $\hat{H}_I = -\mathbf{d} \cdot \mathbf{E} = -d_x E_x = exE_x$, where \mathbf{d} is the atomic dipole operator $\mathbf{d} = q \cdot \mathbf{r}$, with $q = -e$, and \mathbf{r} is the electron's position vector (operator). This interaction term allows transitions between the two levels. The form of the dipole operator can be calculated by using twice the closure relationship $\hat{I} = |g\rangle\langle g| + |e\rangle\langle e|$, that is $\hat{I}(-ex)\hat{I}$; therefore:

$$d_x = -\langle g|ex|g\rangle|g\rangle\langle g| - \langle e|ex|e\rangle|e\rangle\langle e| - \langle g|ex|e\rangle(|g\rangle\langle e| + |e\rangle\langle g|) \equiv -c_+\mathbf{I} + c_-\sigma_z - d_0\sigma_x, \tag{11}$$

with $c_{\pm} = (\langle g|ex|g\rangle \pm \langle e|ex|e\rangle)/2$, $d_0 = \langle g|ex|e\rangle$, and where we have used the matrix representations ($|g\rangle\langle e| + |e\rangle\langle g| \equiv \sigma_x$, $|g\rangle\langle g| \equiv (\mathbf{I} + \sigma_z)/2$, and $|e\rangle\langle e| \equiv (\mathbf{I} - \sigma_z)/2$). We must stress that sometimes, parity arguments [9] narrow the form of the dipole operator, leading up to the expression $d_x = -\langle g|ex|e\rangle(|g\rangle\langle e| + |e\rangle\langle g|) = -d_0\sigma_x$. Likewise, it is customary to introduce the Rabi frequency $\Omega = E_0 d_0/\hbar$. In short, the total Hamiltonian is given by $\hat{H}_0 + \hat{H}_I$, and therefore, the corresponding Schrödinger equation, by using this new variables, is given by:

$$i\hbar \frac{\partial}{\partial t} |\Psi(t)\rangle = \left(\hbar(\bar{\omega} + C_+) \mathbf{I} - \hbar\left(\frac{\omega_0}{2} - C_-\right)\sigma_z + \hbar\Omega\sigma_x \cos \omega t \right) |\Psi(t)\rangle = \hat{H} |\Psi(t)\rangle, \tag{12}$$

with $C_{\pm} = c_{\pm} \cos \omega t$. The general solution of this Schrödinger equation can again be obtained by using a time-dependent linear combination of fundamental and excited states, $|g\rangle \equiv |0\rangle$ and $|e\rangle \equiv |1\rangle$, of the particle, that is $|\Psi(t)\rangle = c_0(t)|0\rangle + c_1(t)|1\rangle$. However, the high value of the frequency ω means that the electric field is rapidly oscillating, which suggests to make the following change $|\Psi(t)\rangle = f_0(t) \exp(i\omega t/2)|0\rangle + f_1(t) \exp(-i\omega t/2)|1\rangle \equiv \exp(i\omega\sigma_z t/2)|\eta(t)\rangle$. Moreover, in many cases, by parity arguments, it is fulfilled that $c_{\pm} = 0$. Therefore, by substituting this state into Equation (12), we obtain the following Hamiltonian for the state $(f_0(t), f_1(t))^T \equiv |\eta(t)\rangle$,

$$\hat{H}'|\eta(t)\rangle \approx \left(\hbar\bar{\omega} \mathbf{I} - \frac{\hbar\delta}{2}\sigma_z + \frac{\hbar\Omega}{2}\sigma_x \right) |\eta(t)\rangle, \tag{13}$$

with $\delta = (\omega_0 - \omega)$ the detuning parameter and where we have neglected terms rapidly oscillating of the form $\exp(\pm i\omega t)$; that is, a temporal Rotating Wave Approximation (RWA) has been made, and a time independent Hamiltonian has thus been obtained. We must stress that under this approximation, the terms C_{\pm} in Equation (12) can be also neglected independently of the wave-function parity. Finally, note that Hamiltonians given by Equations (6) and (13) have the same algebraic structure.

3. Quantum Photonic Simulations

In this section, we present the quantum simulation, which can be implemented by an integrated photonic device, that is integrated optical gratings supporting two collinear guided modes, that is

two mode guides assisted by a periodic perturbation. It can be considered the basic brick for constructing more complex simulators.

3.1. Classical Study of the Photonic Device

Let us consider a standard integrated photonic device consisting of, for example, an integrated waveguide 1D (one-dimensional) with refractive index $n(x)$ (slab guide) that supports two optical modes $e_0(x)$ and $e_1(x)$. These modes are collinear and travel in the z -direction with propagation constants β_0 and β_1 , that is wave vectors in the z -direction defined as $\beta = (\omega/c)N$, where ω is the frequency of the mode and N is the effective index [10]. The mentioned modes are coupled by an integrated grating present in a region of the slab guide, as shown in Figure 1a), where relevant parameters are indicated, that is substrate index n_s , film index n_f , cover index $n_c = 1$, and film thickness d . The grating is represented, for example, by a periodic modulation (perturbation) of the electrical permittivity [10],

$$\Delta\epsilon(x, z) = \Delta\epsilon(x) \cos(\gamma z + \alpha_0), \tag{14}$$

with $\Delta\epsilon(x)$ the modulation strength of the optical grating, α_0 an initial phase, if required, $\gamma = 2\pi/\Lambda$ the frequency of the perturbation, and Λ its period. This index profile can be obtained by different technologies of integrated optics, for instance ion-exchange in glass [15,16] could be used, or even by optical fiber technology [17]. Likewise, in crystals such as lithium niobate, these optical gratings can also be reconfigurable due to acousto-optic or electro-optic effects [18].

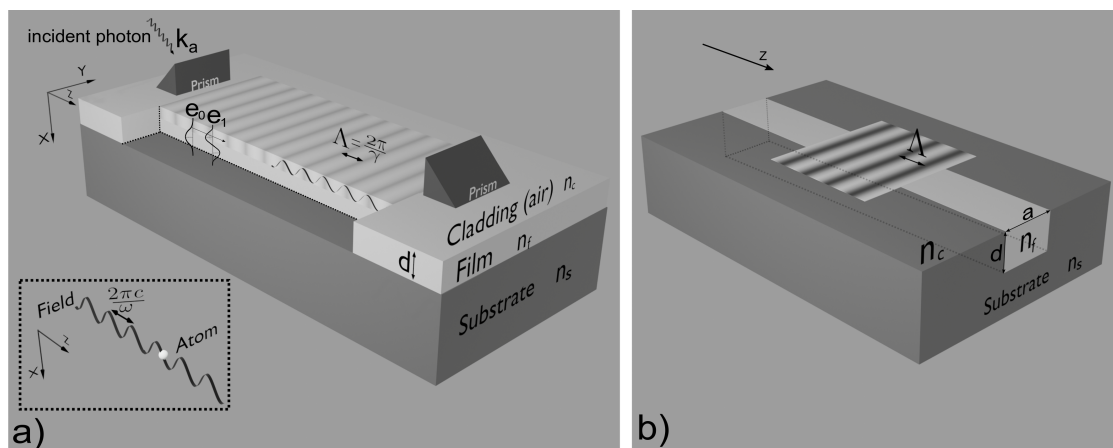


Figure 1. (a) Integrated optical grating with period Λ on a two-mode slab waveguide with modes $e_0(x)$ and $e_1(x)$. The inset shows the simulated mechanical device: atom-field interaction. (b) Integrated optical grating with period Λ on a two-mode channel waveguide with modes, for example $e_{00}(x, y)$ and $e_{10}(x, y)$.

As we assume that only two guided modes are excited in our integrated photonic structure, the perturbed electric field amplitude is given by $e(x, z) = a_0(z)e_0(x) + a_1(z)e_1(x)$. It is well known that the general set of equations that describe the coupling between n copropagating optical modes with propagation constants β_n in a perturbed waveguide and that allow calculating the amplitude coefficients $a_n(z)$ is given by (see for instance [10]):

$$-i \frac{da_n(z)}{dz} = \tilde{\beta}_n(z)a_n(z) + \sum_{n \neq m} C_{nm}(z)a_m(z), \tag{15}$$

where $\tilde{\beta}_n(z) = \beta_n + C_{nn}(z)$ are the corrected propagation constants due to the self-coupling coefficients C_{nn} and C_{nm} are the coupling coefficients between the n mode and each of the other m modes. All these coefficients are calculated as follows [10]:

$$C_{nm}(z) = \frac{\omega}{2} \int \Delta\epsilon(x, z) e_n(x) e_m^*(x) dx, \tag{16}$$

with ω the temporal frequency of the modes and $e_n(x)$ and $e_m(x)$ the normalized optical n and m modes of a planar guide.

The study with 2D guides (integrated channel guides or optical fibers) can be also made, but no new relevant result would be obtained. Indeed, a channel guide can be defined starting from a planar guide whose width is reduced up to a size a of the same order as its depth, that is $a \approx d$, as shown in Figure 1b). In such a case, the optical modes are characterized by two subscripts, one for each spatial direction, that is $e_{np}(x, y)$ and $e_{mq}(x, y)$; therefore, the general coupling coefficients are given by:

$$C_{nppmq}(z) = \frac{\omega}{2} \int \Delta\epsilon(x, y, z) e_{np}(x, y) e_{mq}^*(x, y) dx dy, \tag{17}$$

where we assumed that the grating modulation can also have a y -dependence. Finally, the mode coupling equations can be obtained by applying the formal changes $n \rightarrow np, m \rightarrow mq$ in Equation (15). Accordingly, the results for planar guides can be easily transferred to channel guides.

3.2. Quantum Study of the Photonic Device

A canonical quantization procedure [1,2] proves that the $a(z)$ coefficients become the photon absorption (or emission) operators $\hat{a}(z)$ (correspondence principle). Therefore, the coupled mode equations are in fact the Heisenberg equations, which, in general, give the evolution of the operators in time. In this case, they give the spatial evolution of the operators. Moreover, the relevant operator here responsible for the spatial propagation of quantum states of the device is the momentum operator, which is the generator of spatial translations [2,19], and not the Hamiltonian, which is the generator of temporal translations. In short, we can study the integrated photonic device in a fully quantum mechanical way, by solving the equations for absorption operators (spatial Heisenberg equations). That is, by performing the change $a(z) \rightarrow \hbar\hat{a}(z)$ in Equation (15), we obtain [2,20]:

$$-i\hbar \frac{d\hat{a}_n(z)}{dz} = \hbar\tilde{\beta}_n\hat{a}_n(z) + \hbar \sum_{n \neq m} C_{nm}(z)\hat{a}_m(z). \tag{18}$$

We must stress that modal coupling preserves energy; therefore, Equation (18) corresponds to a unitary transformation, and accordingly, $C_{nm} = C_{mn}$. On the other hand, we only consider single-photon states, which is enough for our simulation purposes. We must stress that the linear momentum of a single photon without modal coupling, that is $\Delta\epsilon(x, y) = 0$, is given by $p_{(0,1)} = \hbar\beta_{(0,1)}$ depending on whether the photon is excited in mode β_0 or mode β_1 [19,20]. Obviously, more general quantum states could be used such as multiphoton states, entangled states of two photons, and so on. These states would give rise to more complex quantum simulations, which fall outside of the scope of this work. In general, the single-photon state is a quantum superposition because the photon can either be excited in the mode β_0 , that is $|1_0\rangle$, or in the mode β_1 , that is $|1_1\rangle$. Hence, the general quantum state is given by:

$$|L(z)\rangle = a_0(z)|1_0\rangle + a_1(z)|1_1\rangle, \tag{19}$$

where $a_0(z)$ and $a_1(z)$ are the quantum complex amplitudes and fulfil the normalization condition $|a_0(z)|^2 + |a_1(z)|^2 = 1$. States $|1_0\rangle$ and $|1_1\rangle$ must be understood as single-photon states at a distance (plane) z . It can be checked that the solutions of Equation (18) for the spatial propagation of emission operators are the same as for single-photon states $|L(z)\rangle$ [21]. The main reason is that

single-photon states are proportional to emission operators, that is $|1_0\rangle = \hat{a}_0^\dagger|0\rangle$, $|1_1\rangle = \hat{a}_1^\dagger|0\rangle$. Indeed, let us consider free propagation, that is non-coupling case $C_{nm} = 0$, then the solutions of Equation (18) are $\hat{a}_{0,1}(z) = \exp(i\beta_{0,1}z)\hat{a}_{0,1}(0)$. Now, let us consider, for the sake of simplicity, a single-photon state at $z = 0$, for instance $|1_0\rangle$, then the optical propagation can be obtained as follows: $|1_0\rangle = \hat{a}_0^\dagger(0)|0\rangle$ (one-photon emission), but by taking into account the z -propagation, we have $|L(z)\rangle = \exp(i\beta_0z)\hat{a}_0^\dagger(z)|0\rangle = \exp(i\beta_0z)|1_0\rangle \equiv a_0(z)|1_0\rangle$; therefore, the coefficients $a_{0,1}(z)$ of a single-photon state have the same optical propagation solution as the operators $\hat{a}_{0,1}(z)$. This can be proven for a general unitary transformation after a certain algebra. We will take advantage of this property for simulation purposes. Accordingly, for single-photon states, Equation (18) can formally be rewritten as follows:

$$i\hbar \frac{d|L(z)\rangle}{dz} = -\hbar \begin{pmatrix} \tilde{\beta}_0(z) & C_{12}(z) \\ C_{21}(z) & \tilde{\beta}_1(z) \end{pmatrix} |L(z)\rangle = -\hat{M}(z)|L(z)\rangle, \tag{20}$$

where $|L(z)\rangle$ is given, in vector representation, by $(a_0(z), a_1(z))^T$ and \hat{M} is the matrix representation of the so-called momentum operator. This is equivalent to the matrix equation given by Equation (2) for the Hamiltonian. We must stress that Equations (2), (3), (13), (18) and (20) are the main results for implementing the quantum simulations in this work.

3.3. Photonic Simulation of Spin-Magnetic Field Interaction

Let us consider an integrated optical grating characterized by the function given by Equation (14). It will be useful to work with the slowly varying operators \hat{A}_n , defined as $\hat{A}_n = \hat{a}_n \exp(-i\beta_n z)$. On the other hand, the coupling coefficients for a grating with initial phase $\alpha_0 = 0$ can be written as $C_{00} = c_{00} \cos \gamma z$, $C_{11} = c_{11} \cos \gamma z$, and $C_{01} = C_{10} = C_o \cos \gamma z$, where $c_{nm} = (\omega/2) \int \Delta\epsilon(x) e_n(x) \cdot e_m^*(x) dx$, and so on. Therefore, from Equation (18), we obtain, for the two-mode case, the following spatial Heisenberg equations:

$$i \frac{d\hat{A}_0(z)}{dz} = -\hat{A}_0 c_{00} \cos \gamma z - \hat{A}_1 \frac{C_o}{2} e^{-i\Delta\beta_{01}z} [e^{i\gamma z} + e^{-i\gamma z}], \tag{21}$$

$$i \frac{d\hat{A}_1(z)}{dz} = -\hat{A}_1 c_{11} \cos \gamma z - \hat{A}_0 \frac{C_o}{2} e^{i\Delta\beta_{01}z} [e^{i\gamma z} + e^{-i\gamma z}], \tag{22}$$

where $\Delta\beta_{01} = \beta_0 - \beta_1$. The above equation reveals that we have oscillating terms coming from the cosine of the self-coupling terms with arguments $\pm\gamma z$ and also terms with arguments $(\gamma - \Delta\beta_{01})z$ and $(\gamma + \Delta\beta_{01})z$. We make the assumption that γ is of the same order as $\Delta\beta_{01}$, so that $(\gamma - \Delta\beta_{01})$ is small. The other terms are rapidly oscillating and, thus, will average to zero on a sufficiently large z -scale. We must stress that what we do here is essentially a spatial RWA, which is well-known in light-matter interaction in the time domain. Therefore, the above equations become, to a good approximation,

$$i \frac{d\hat{A}_0(z)}{dz} = -\hat{A}_1 \frac{C_o}{2} \exp[-i(\Delta\beta_{01} - \gamma)z], \tag{23}$$

$$i \frac{d\hat{A}_1(z)}{dz} = -\hat{A}_0 \frac{C_o}{2} \exp[i(\Delta\beta_{01} - \gamma)z]. \tag{24}$$

Next, we make the following relabeling $\Delta\beta_{01} \equiv \Delta\beta$ and define the new absorption operators $\hat{A}_0 = \hat{b}_0 \exp(-i\Delta\beta z/2)$ and $\hat{A}_1 = \hat{b}_1 \exp(i\Delta\beta z/2)$. We rewrite the Heisenberg equations in terms of the $\hat{b}(z)$ operators,

$$i \frac{d\hat{b}_0}{dz} = -\frac{\Delta\beta}{2} \hat{b}_0 - \frac{C_o}{2} \hat{b}_1 \exp(i\gamma z), \tag{25}$$

$$i \frac{d\hat{b}_1}{dz} = \frac{\Delta\beta}{2} \hat{b}_1 - \frac{C_o}{2} \hat{b}_0 \exp(-i\gamma z). \tag{26}$$

It is interesting to note that $\hat{a}_{0,1}$ and $\hat{b}_{0,1}$ are, after the spatial RWA, the same operators, except a global phase, that is $\hat{a}_{0,1} = b_{0,1} \exp(i\bar{\beta}z)$, $\bar{\beta} = (\beta_0 + \beta_1)/2$. Finally, as mentioned above, we can write the above equation in a matrix form acting on the single-photon state $|L_b(z)\rangle = b_0(z)|1_0\rangle + b_1(z)|1_1\rangle$, where $|L(z)\rangle = |L_b(z)\rangle \exp(i\bar{\beta}z)$, that is,

$$i\hbar \frac{\partial}{\partial z} |L_b(z)\rangle = -\frac{\hbar}{2} \begin{pmatrix} \Delta\beta & C_o \exp(i\gamma z) \\ C_o \exp(-i\gamma z) & -\Delta\beta \end{pmatrix} |L_b(z)\rangle = -\frac{\hbar}{2} \mathbf{B} \begin{pmatrix} \cos \alpha & \sin \alpha \exp(i\gamma z) \\ \sin \alpha \exp(-i\gamma z) & -\cos \alpha \end{pmatrix} |L_b(z)\rangle = -\hat{M}(z) |L_b(z)\rangle, \tag{27}$$

with $\cos \alpha = \Delta\beta/B$, $\sin \alpha = C_o/B$, and $B = \sqrt{\Delta\beta^2 + C_o^2}$. This equation is just the spatial equivalent of Equation (2). A Hamiltonian operator is replaced by a momentum operator. Obviously, the dynamic properties are identical under the formal changes: $\omega \leftrightarrow \gamma$, $\gamma_p B_o \leftrightarrow B$, $\theta \leftrightarrow \alpha$. Note that a rotating equivalent vector $(\gamma_p \mathbf{B})_{eq} \equiv \mathbf{B} = B(\sin \alpha \cos \gamma z, -\sin \alpha \sin \gamma z, \cos \alpha)$ is obtained. In short, we have achieved a photonic simulator of spin-magnetic field coupling. However, we must stress some limitations for this simulator. The momentum operator \hat{M} defined by (27) and simulating the coupling spin-magnetic field only is valid under the spatial RWA, that is the values of $\Delta\beta$ and γ have to be high and not too different. Therefore, we will be able to simulate the interaction with magnetic fields with a large z-component and oscillating with a frequency ω of the same order as the term $\gamma_p B_o \cos \theta$.

Finally, it is interesting to obtain a constant momentum operator by applying a unitary transformation (rotating reference system) to the quantum state $|L_b(z)\rangle$, that is,

$$|l(z)\rangle = \hat{U}(z, \gamma) |L_b(z)\rangle = \exp(-i\gamma\sigma_z z/2) |L_b(z)\rangle. \tag{28}$$

Therefore, by using $|L_b(z)\rangle = \exp(i\gamma\sigma_z z/2) |l(z)\rangle$ in Equation (27), we obtain, after a certain, but straightforward calculation, the following momentum operator for the state $|l(z)\rangle$:

$$-\hat{M}' |l(z)\rangle = \frac{\hbar}{2} \begin{pmatrix} -\Delta\beta + \gamma & -C_o \\ -C_o & \Delta\beta - \gamma \end{pmatrix} |l(z)\rangle = -\frac{\hbar}{2} D_o \begin{pmatrix} \cos \alpha' & \sin \alpha' \\ \sin \alpha' & -\cos \alpha' \end{pmatrix} |l(z)\rangle, \tag{29}$$

where $\cos \alpha' = (\Delta\beta - \gamma)/D_o$, $\sin \alpha' = C_o/D_o$, and $D_o = \sqrt{(\Delta\beta - \gamma)^2 + C_o^2}$. As shown later, these results are important for simulating both dynamical and topological properties. By comparison between Equations (5) and (29), we obtain the following simulation parameters:

$$(\omega - \gamma_p B_o \cos \theta) \leftrightarrow (\Delta\beta - \gamma), \quad \gamma_p B_o \sin \theta \leftrightarrow C_o. \tag{30}$$

Next, it is interesting to compute the eigenstates $|l(z)\rangle$ and eigenvalues β_l of the momentum operator \hat{M}' given by Equation (6), that is $|l(z)\rangle = \exp(\frac{i}{\hbar} p_l z) |l(0)\rangle = \exp(i\beta_l z) |l(0)\rangle$. After a standard calculation, we have:

$$|l_+(0)\rangle = \cos \frac{\alpha'}{2} |1_0\rangle + \sin \frac{\alpha'}{2} |1_1\rangle, \quad |l_-(0)\rangle = \sin \frac{\alpha'}{2} |1_0\rangle - \cos \frac{\alpha'}{2} |1_1\rangle, \tag{31}$$

with eigenvalues $\beta_{\pm} = \pm D_o/2$, that is linear momentums $p_{\pm} = \pm \frac{\hbar}{2} D_o = \pm p_o$. Therefore, by taking into account Equation (28), the full evolved states $|L_b(z)\rangle$ can be easily obtained. Note that we are simulating the quantum state $\Psi(t)$ given by Equation (4), and thus, for example, quantum processing based on NMR could be simulated by this photonic device. For the sake of expositional convenience, we will return to this question in the next subsection.

3.4. Photonic Simulation of Light-Matter Interaction

For the case of light-matter interaction, we have a more direct photonic simulation by using a two-mode planar guide perturbed by an integrated optical grating. Thus, by defining $\Delta\beta = \beta_0 - \beta_1$ and $\bar{\beta} = (\beta_0 + \beta_1)/2$ and for the sake of simulation purposes, choosing an initial phase $\alpha_0 = \pi$, the momentum operator defined in Equation (20) can be rewritten as follows:

$$\hat{M}|L(z)\rangle = \hbar \left[(\bar{\beta} + C_+) \mathbf{I} + \left(\frac{\Delta\beta}{2} - C_- \right) \sigma_z - C_o \cos(\gamma z) \sigma_x \right] |L(z)\rangle, \tag{32}$$

where $C_{\pm} = (C_{00}(z) \pm C_{11}(z))/2$. As in the mechanical case, these terms could be zero if the optical modes $e_{n,m}(x)$ and perturbation $\Delta\epsilon(x)$ have a suitable parity, that is even or odd modes along with an odd perturbation. Next, we perform the following relevant change in the vector representation of the single-photon state $|L(z)\rangle \equiv (l_0(z) \exp(i\gamma z/2), l_1(z) \exp(-i\gamma z/2))^t \equiv \exp(i\gamma\sigma_z z/2) |l(z)\rangle$, with t indicating the transpose. By inserting this state into the above equation, using $\hat{M} = -i\hbar\partial/\partial z$, and neglecting terms that are rapidly oscillating, that is $\exp(\pm iq\gamma z)$ with $q = 1/2, 1, 3/2$, the following momentum operator is obtained for the state $|l(z)\rangle \equiv (l_0(z), l_1(z))^t$:

$$\hat{M}'|l(z)\rangle \approx \left(\hbar\bar{\beta} \mathbf{I} + \frac{\hbar\delta_s}{2} \sigma_z - \frac{\hbar C_o}{2} \sigma_x \right) |l(z)\rangle, \tag{33}$$

with $\delta_s = \Delta\beta - \gamma$. This momentum operator simulates the Hamiltonian given by Equation (13), where the following simulation parameters are obtained:

$$\bar{\omega} \leftrightarrow -\bar{\beta}, \quad \delta = (\omega_0 - \omega) \leftrightarrow \delta_s = (\Delta\beta - \gamma), \quad \Omega \leftrightarrow C_o, \tag{34}$$

with $\delta \leftrightarrow \delta_s$ the detuning simulation parameter and $\Omega \leftrightarrow C_o$ the Rabi frequency simulation parameter. Hence, this photonic device simulates light-matter interaction under a spatial RWA. Obviously, all temporal dynamics obtained by light-matter interaction can be simulated by means of this photonic device, as for example Rabi oscillations, logic gates for one-qubit transformations, and so on. In order to make clear these possibilities, let us consider the synchronous (or resonant) case, that is $\Delta\beta = \gamma$. The momentum operator is thus simplified, and the solutions can be easily obtained. In matrix form, the solution of the equation above is given by:

$$\begin{pmatrix} l_0(z) \\ l_1(z) \end{pmatrix} = \begin{pmatrix} \cos \frac{C_o}{2} z & -i \sin \frac{C_o}{2} z \\ -i \sin \frac{C_o}{2} z & \cos \frac{C_o}{2} z \end{pmatrix} \begin{pmatrix} l_0(0) \\ l_1(0) \end{pmatrix} \equiv X(\Theta/2) \begin{pmatrix} l_0(0) \\ l_1(0) \end{pmatrix}, \tag{35}$$

with $\Theta = C_o z$ and where an irrelevant global phase $e^{i\bar{\beta}z}$ has been omitted. As a simple example, if we choose a length of the grating (interaction length) $z = 2\pi/C_o$, then a Xquantum logic gate is implemented. We must stress that these are transformations corresponding to the so-called Θ -pulses in atom-light temporal interaction for computing purposes [22]. For example, given an input state $|1_0\rangle$, the state propagating along the optical grating will be:

$$|L(z)\rangle = l_0(z)|1_0\rangle + l_1(z)|1_1\rangle. \tag{36}$$

On the other hand, for the case $|\delta_s| \ll C_o$ and by omitting again the global phase $e^{i\bar{\beta}z}$, we obtain, as a solution to Equation (33), a phase gate, that is,

$$\begin{pmatrix} l_0(z) \\ l_1(z) \end{pmatrix} = \begin{pmatrix} \exp(i\frac{\delta_s}{2}z) & 0 \\ 0 & \exp(-i\frac{\delta_s}{2}z) \end{pmatrix} \begin{pmatrix} l_0(0) \\ l_1(0) \end{pmatrix} \equiv Z(\Phi/2), \tag{37}$$

where $\Phi = \delta_s z$. Therefore, a Z quantum logic gate is obtained from Equation (37) if $\delta_s z/2 = \pi/2$, an S-gate if $\delta_s z/2 = \pi/4$, a T-gate if $\delta_s z/2 = \pi/8$, and so on. Moreover, by using an optical grating

implementing a transformation $X(\Theta/2)$ and two phase gates $Z(\Phi/2)$, a ZXZ-factorization of $SU(2)$ is obtained; therefore, any unitary transformation can be implemented with the photonic device, and consequently, any one-qubit can be generated.

Next, we present solutions for the asynchronous case, that is $\Delta\beta \neq \gamma$, which provides a most general solution and will be very useful to obtain geometric phases. By using standard methods to solve a linear equation system, the general solution of Equation (33) is given by:

$$\begin{pmatrix} l_0(z) \\ l_1(z) \end{pmatrix} = \begin{pmatrix} \cos \frac{\delta_r}{2} z + i \frac{\delta_s}{\delta_r} \sin \frac{\delta_r}{2} z & -i \frac{C_0}{\delta_r} \sin \frac{\delta_r}{2} z \\ -i \frac{C_0}{\delta_r} \sin \frac{\delta_r}{2} z & \cos \frac{\delta_r}{2} z - i \frac{\delta_s}{\delta_r} \sin \frac{\delta_r}{2} z \end{pmatrix} \begin{pmatrix} l_0(0) \\ l_1(0) \end{pmatrix}, \quad (38)$$

with $\delta_r = \sqrt{\delta_s^2 + C_0^2}$ and where, once more, the irrelevant global phase $e^{i\beta z}$ is omitted. Note that for $\delta_s = 0$, the matrix given by Equation (35) is recovered. Likewise, under the condition $|\delta_s| \ll C_0$, the matrix solution given by Equation (37) is obtained. We must recall that all these transformations are obtained in a spatial rotating reference system defined by Equation (28) and induced by the RWA approximation, as occurs in atom-light temporal interactions. Likewise, we must stress that by using the simulation parameters given by Equation (34), mechanical solutions for light-matter (atom) interaction are directly obtained. Finally, it is also easy to check that the same solutions are obtained for the spin-magnetic field interaction simulation given by Equation (29); therefore, such an interaction has the same quantum processing properties as the atom-optical field interaction.

Finally, it is worth paying attention to the problem of properly initializing a quantum state. For that, let us consider an SPDC (Spontaneous Parametric Down Conversion) source of biphotons $|1_{k_a} 1_{k_b}\rangle$, that is twin photons excited in two spatial modes propagating along directions k_a and k_b . Photon $|1_{k_b}\rangle$ is directed towards an APD device, and the other one $|1_{k_a}\rangle$ is directed to the prism-waveguide coupler, as shown in Figure 1a). The direction k_a is chosen in such a way that, for example, if the fundamental mode of the planar guide is excited, that is $k_a = k_0$, then we obtain the single-photon state (or register) $|1_0\rangle$. Alternatively, direction $k_a = k_1$ can be chosen to excite the mode e_1 of the planar guide, and thus, the single-photon state (or register) $|1_1\rangle$ is obtained. If we had channel waveguides, a similar procedure can be used, for example before the channel waveguide, there would be a planar waveguide with a prism-waveguide coupler and, next, an integrated lens or a similar integrated optical element [15] in such a way that the excited mode is focused onto the channel waveguide to excite the desired single-photon state. Next, by using optical gratings, different quantum transformations can be performed, and consequently, a general output state $|L\rangle = a_0(z)|1_{k_0}\rangle + a_1(z)|1_{k_1}\rangle$ is obtained. Finally, at a distance z , another prism-waveguide coupler can be placed at the end of the device to detect the quantum state. Photon detections can be made by using coincidences between the output photon and the photon $|1_{k_b}\rangle$ reaching the APD.

3.5. Implementation of Photonic Simulators

In this subsection, we present more complex simulators by using several integrated optical gratings along with other integrated components as Directional Couplers (DCs) made with Single-Mode (SMWs) or Two-Mode channel Waveguides (TMWs). We present a simulator of the interaction between an atom with four levels and Θ -pulses, next the interaction of a particle (or physical system) with spin 3/2 and a magnetic field, and finally, an arbitrary unitary transformation $SU(4)$ implemented with optical gratings what allows reducing the number of paths by half or even to a quarter, which can be generalized to $SU(N)$ transformations, which can be of interest for photonic simulators.

Let us consider, as the first example, the Optical Grating (OG) studied above, but with a number $d = 4$ of collinear guided modes whose propagation constants are β_j with $j = 1, 2, 3, 4$. This simple device can simulate a four-level atom, which can be used to implement a CNOT logic gate operation under atom-laser interaction [22]. The optical grating fulfills $\gamma = \beta_2 - \beta_3$; therefore, it will produce an efficient transition between Modes 2 and 3 if $z = \pi/C_0$ (π -pulse in atom-laser interaction) according to

Equation (35). We can identify each single-photon state excited in each optical mode as a computational state (two-qubit single-photon [23]); thus, we have the state $|L\rangle = c_{00}|00\rangle + c_{01}|01\rangle + c_{10}|10\rangle + c_{11}|11\rangle$. When this state goes through the optical grating, the output state is $|L\rangle = c_{00}|00\rangle + c_{01}|01\rangle + c_{11}|10\rangle + c_{10}|11\rangle$, that is a CNOT operation is obtained. Obviously, this is not the best way to implement logic gates for two-qubits, but it makes clear how OGs can be used to simulate interaction between an atom with several levels and the so-called Θ -pulses.

The second example consists of using single-mode channel guides coupled by OGs in order to simulate the interaction between a particle (or physical system) with spin s and a magnetic field. This can be implemented by using a number $N=2s+1$ of optical modes excited in N channel waveguides and coupled by OGs, as shown in Figure 2 for the particular case of four guides (spin $s=3/2$). We must stress that coupling between parallel SMWs can be also described by the Heisenberg quantum equations given by Equation (18). In order to simulate spin-magnetic field interaction, either the strength of the OGs or the separation between consecutive SMWs has to be adjusted, and therefore, proper coupling strength values $C_{j,j+1}$ with $j=1, \dots, N-1$, between consecutive guides, are obtained. Likewise, the SMWs have to be designed with different propagation constants β_j (asynchronous guides) by changing, for example, the depth of each channel waveguide. Finally, it is well known in integrated optics that for asynchronous DCs assisted by optical gratings, the coupling due to the overlapping fields is negligible. As a particular example, let us consider spin $s = 3/2$. The general equation system is given by:

$$-i\hbar \frac{d\hat{a}_j(z)}{dz} = \hbar\tilde{\beta}_j(z)\hat{a}_j(z) + \hbar \sum_{j' \neq j} C_{jj'}(z)\hat{a}_{j'}(z). \tag{39}$$

with $(|j - j'| < 2)$, that is coupling only exists between consecutive channel guides. Next, by using the same procedure followed for the case of spin-1/2, we obtain, after a long, but straightforward calculation, the following equation system:

$$-i\hbar \frac{\partial}{\partial z} |L_b(z)\rangle = -\Delta_o \mathbb{I}_{4 \times 4} + \begin{pmatrix} 3\Delta_o & C_{12} \exp(i\gamma z) & 0 & 0 \\ C_{21} \exp(-i\gamma z) & \Delta_o & C_{23} \exp(i\gamma z) & 0 \\ 0 & C_{32} \exp(-i\gamma z) & -\Delta_o & C_{34} \exp(i\gamma z) \\ 0 & 0 & C_{43} \exp(-i\gamma z) & 3\Delta_o \end{pmatrix} |L_b(z)\rangle \tag{40}$$

where $\mathbb{I}_{4 \times 4}$ is the identity matrix and the following propagation constants are used: $\beta_1, \beta_2 = \beta_1 - \Delta_o, \beta_3 = \beta_1 - 2\Delta_o, \beta_4 = \beta_1 - 3\Delta_o$. These values can be achieved by adjusting, for example, the width of the channel waveguides. On the other hand, the coupling coefficients for the gratings fulfil the relationships $C_{12} = C_{21} = C_{34} = C_{43} = \sqrt{3}C_o$ and $C_{23} = C_{32} = 2C_o$, which can be achieved by adjusting the separation between consecutive guides with optical modes $e_j(x, y), j=1, 2, 3, 4$. In our case, Guides 2–3 are closer than 1–2 and 3–4 because the coupling between Guides 2 and 3 is larger, as shown in Figure 2. Finally, by defining $\cos \theta = \Delta_o / \Gamma$ and $\sin \theta = C_o / \Gamma$, with $\Gamma = (\Delta_o^2 + C_o^2)^{1/2}$, and a fictitious magnetic field $\mathbf{B}_f = (\sin \theta \cos \gamma z, -\sin \theta \sin \gamma z, \cos \theta)$, we can write the above equation system as follows:

$$-i\hbar \frac{\partial}{\partial z} |L_b(z)\rangle = \{-\hbar\Delta_o \mathbb{I}_{4 \times 4} + \frac{\hbar}{2} \Gamma \mathbf{J}(3/2) \mathbf{B}_f\} |L_b(z)\rangle \tag{41}$$

where $\mathbf{J}(3/2) = (J_x(3/2), J_y(3/2), J_z(3/2))$ are the spin matrices for spin $s = 3/2$. In short, we constructed a photonic simulator for interaction between a spin-3/2 particle, or physical system, and a periodic magnetic field.

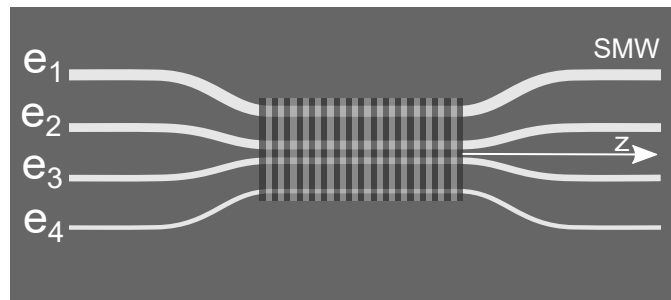


Figure 2. Four non-synchronous Single-Mode channel Waveguides (SMWs) assisted by an optical grating to simulate the interaction between a spin $s = 3/2$ particle and an oscillating magnetic field.

Next, we present a general unitary transformation $SU(4)$ by using optical gratings. With this example, we want to show that OGs allow reducing the number of paths required for constructing a simulator. Indeed, an $SU(4)$ simulator is formed by four paths implemented by SMWs with optical modes $e_{00}^{(j)}(x, y)$ ($j=1, \dots, 4$), six DCs, and six Phase Shifters (PSs), as shown in Figure 3 (bottom). However, if OGs are used, we only need two paths, that is TMWs with modes $e_{00}^{(j)}(x, y)$, $e_{10}^{(j)}(x, y)$ ($j = 1, 2$) and six OGs, as shown in Figure 3 (up). In this case, we also use Selective Directional Couplers (SDCs) (a SDC always performs an X transformation in one mode, and the other mode undergoes an identity transformation). Note that the number of paths was reduced by half because OGs act on collinear modes, unlike directional couplers, which act on codirectional modes. Obviously, if we had used OGs with four modes, we could reduce the number of paths by $1/4$. Overall, we will be able to reduce the number of paths by $1/d$ if we use OGs with a number d of collinear modes. Ultimately, we can take advantage of the OGs to increase integration and thus to implement more flexible and scalable photonic simulators such as for example boson sampling ones [24], where the number of paths would be reduced by half. In short, the number N of paths of any required $SU(N)$ transformation [25] could be reduced up to N/d .

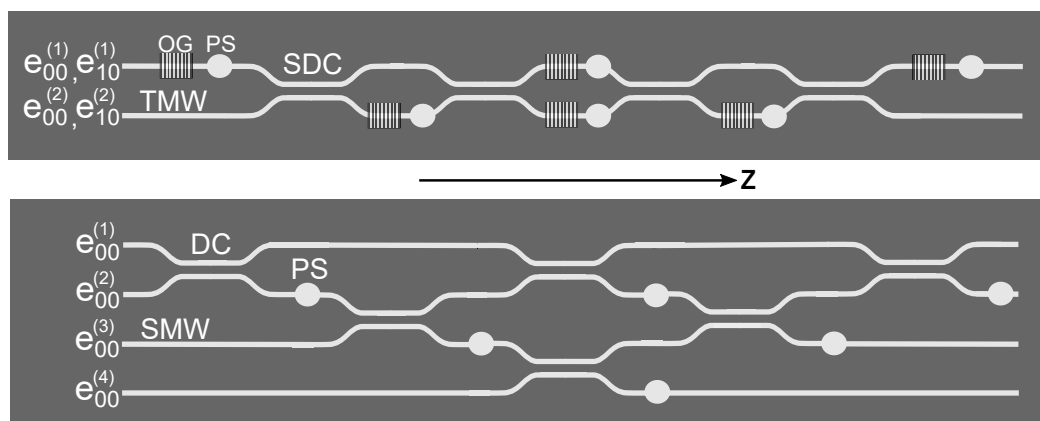


Figure 3. Standard implementation (bottom) of an arbitrary unitary transformation $SU(4)$ by using Single-Mode channel Waveguides (SMWs) and Directional Couplers (DCs) (bottom). Alternative implementation (top) by using Two-Mode channel Waveguides (TMWs), Selective Directional Couplers (SDCs) and Optical Gratings (OGs). PS, Phase Shifter.

Finally, it is important to indicate that quantum photonic devices have their own limitations [4]. Thus, the difficulty to implement two-qubit logic gates is well known, which is, at present, an important drawback in general purpose quantum photonic computation. However, quantum photonic simulation, or simply quantum photonic computation, for specific purposes can provide efficient technological

solutions, particularly if new degrees of freedom are incorporated. In our case, we have just shown that integrated OGs allow processing with several collinear modes, which improves the optical integration for high-dimensional problems, that is it provides a moderate increase of the on-chip flexibility and scalability for photon-based quantum simulation. Moreover, OGs enable simulating quantum devices under variable perturbations and, in particular, periodic perturbations, which usually appear in quantum systems interacting with fields like spin ($N=2s+1$ modes)-magnetic field interaction, atom (d modes)-optical field interaction, and so on.

4. Quantum Geometric Phases

So far, we have simulated the dynamics of the spin-magnetic and light-matter interaction systems with a photonic device. However, these quantum devices also generate topological or geometric phases besides the dynamic phases. Geometric phases are precisely due to geometric properties as was originally proven by Berry in his seminal work about an adiabatic quantum system [26]. Later, these geometric phases were generalized by Aharonov and Anandan [27] to non-adiabatic processes, and their calculation is made by using the geometric properties of the projective Hilbert space. Finally, a useful extension to geometric phases associated with non-cyclic circuits on the projective Hilbert space was also proposed [28]. On the other hand, topological phases in optics have also been extensively studied in bulk devices with polarization modes [29] and also in integrated optics with spatial modes [30]. At present, geometrical phases have regained interest for their possible application to geometric quantum computation [31,32]. Non-adiabatic spatial propagation on the Hilbert space generate the geometric phase known as the Aharonov–Anandan (AA) phase. It is well known that the spin-magnetic field interaction, as for example NMR, produces AA phases. We must stress that the geometric phase for a two-dimensional projective Hilbert space can be calculated in a geometric way as $\phi_g = (1/2)\Omega(\mathcal{C})$, where $\Omega(\mathcal{C})$ is the solid angle subtended by the circuit \mathcal{C} followed by the quantum state on the Bloch sphere. In this section, we prove that quantum geometrical phases can be obtained by an integrated photonic grating, and therefore, it simulates the geometric phases produced by both a spin-magnetic field system and an atom-optical field system.

4.1. Geometric Phases in Spin-Magnetic Field Photonic Simulation

Let us consider the eigenstates $|l_{\pm}(0)\rangle$ given by Equation (31). Spatial propagation of these states is given, according to Equations (28) and (31), by $|L_b(z)\rangle \equiv |L_{\pm}(z)\rangle = \exp(i\gamma\sigma_z z/2)|l_{\pm}(z)\rangle = \exp(\frac{ip_{\pm}}{\hbar}z) \exp(i\gamma\sigma_z z/2)|l_{\pm}(0)\rangle$. For instance, let us take $|L_+(z)\rangle$ after a propagation distance $z = \nu\Lambda$, that is for a photonic integrated grating with a length $\nu\Lambda$, where $\Lambda = 2\pi/\gamma$ and ν is the number of cycles taken, then we have:

$$|L_+(\nu\Lambda)\rangle = \exp\left(\frac{ip_+}{\hbar}\nu\Lambda\right) \left(\cos\frac{\alpha'}{2} \exp(i\nu\pi)|1_0\rangle + \sin\frac{\alpha'}{2} \exp(-i\nu\pi)|1_1\rangle \right) \tag{42}$$

By following the same procedure for the state $|L_-(z = \nu\Lambda)\rangle$ and taking into account that ν is an integer, we obtain:

$$|L_{\pm}(\nu\Lambda)\rangle = \exp\left(\frac{ip_{\pm}}{\hbar}\nu\Lambda \pm i\nu\pi\right) |l_{\pm}(0)\rangle = \exp(i\phi^{\pm}) |l_{\pm}(0)\rangle. \tag{43}$$

The phases ϕ^{\pm} obtained above are the full phases acquired by the states $|L_{\pm}\rangle$ after ν cycles in the optical grating, that is,

$$\phi^{\pm} = \nu(\pm p_0\Lambda/\hbar \pm \pi) \tag{44}$$

A photonic Bloch sphere is shown on the left in Figure 4 where each point corresponds to a single-photon state given by Equation (19). For comparison purposes, an NMR Bloch sphere is also shown on the right. A single-photon state propagating along z can be represented by the following general expression $|L(z)\rangle = c_0(z)|1_0\rangle + c_1(z)|1_1\rangle$; therefore, each point (x, y, z) of the photonic Bloch

sphere is defined as follows: $x = 2 \operatorname{Re}c_0(z)c_1(z)$, $y = 2 \operatorname{Im}c_0(z)c_1(z)$, $z = |c_0(z)|^2 - |c_1(z)|^2$, where Re and Im stand for real and imaginary parts, respectively.

It is easy to check that eigenstates $|L_{\pm}(z)\rangle$ follow the curves C_c and C'_c corresponding to spherical caps, as shown in Figure 4. The solid angle subtended by a spherical cap with an angular extension α' is given by $\Omega(C) = 2\pi(1 - \cos \alpha')$.

As the full phase ϕ can be decomposed into a dynamical part ϕ_d and a geometric one ϕ_g , then the geometric phase can be obtained from the relationship:

$$\phi_g^{\pm} = \phi_{\pm} - \phi_d^{\pm} \tag{45}$$

We first compute the dynamical phase, that is $\phi_d^{\pm} = \frac{1}{\hbar} \int_0^{\nu\Lambda} \langle L_{\pm}(z) | \hat{M}(z) | L_{\pm}(z) \rangle dz$; therefore, by taking into account the transformation (28) and expression (29) for \hat{M}' , we obtain:

$$\begin{aligned} \phi_d^{\pm} &= \frac{1}{\hbar} \int_0^{\nu\Lambda} \langle L_{\pm}(z) | \hat{M}(z) | L_{\pm}(z) \rangle dz = \frac{1}{\hbar} \int_0^{\nu\Lambda} \langle l_{\pm}(0) | \hat{M}(0) | l_{\pm}(0) \rangle dz = \\ &= \frac{1}{\hbar} \int_0^{\nu\Lambda} (\langle l_{\pm}(0) | \hat{M}' | l_{\pm}(0) \rangle - \frac{\gamma}{2} \langle l_{\pm}(0) | \sigma_z | l_{\pm}(0) \rangle) dz = \\ &= \frac{E_{\pm}}{\hbar} \nu\Lambda \pm \nu\pi \cos \alpha', \end{aligned} \tag{46}$$

and by taking into account the total phase given by Equation (43), the geometrical phases acquired by the eigenstates are given by:

$$\phi_g^{\pm} = \pm \nu\pi(1 - \cos \alpha') = \pm \nu\pi \left(1 - \frac{\Delta\beta - \gamma}{\sqrt{(\Delta\beta - \gamma)^2 + C_0^2}} \right). \tag{47}$$

Note that the geometric phase is half the solid angle subtended by the circuit, where the sign \pm depends on the direction of rotation followed by the state on the Bloch sphere. The corresponding spherical cap circuits C_c and C'_c are shown in Figure 4. Moreover, the geometric phase depends on the device parameters, that is $\Delta\beta, \gamma, C_0$. Likewise, it is important to indicate that the dynamical phase is of order ω^1 (note that $\beta \propto \omega$), but the geometrical phase is of order ω^0 ; therefore, the geometric phase is less sensitive to errors in the distance propagation.

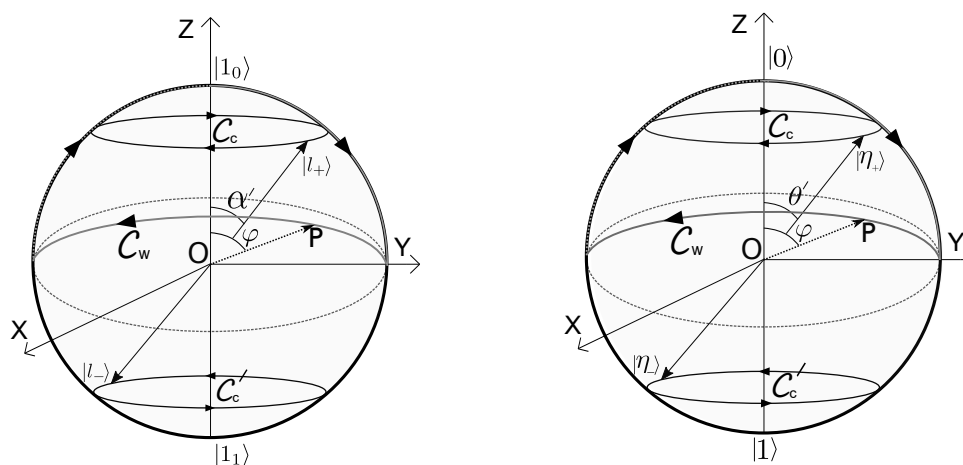


Figure 4. On the left, a photonic Bloch sphere shows the evolution of the single-photon states $|l_+\rangle$ and $|l_-\rangle$ (spherical cap circuits C_c and C'_c). Likewise, a spherical wedge circuit C_w is shown. On the right, the simulated mechanical Bloch sphere for an interacting atom-field system is shown, with similar spherical cup circuits for states $|\eta_+\rangle$ and $|\eta_-\rangle$ and also a spherical wedge circuit C_w .

In short, a single-photon state acquires an AA geometric phase under propagation in an integrated photonic grating. The same expression is found for a spin-1/2 particle in a magnetic field; therefore, topological simulations can be made. Thus, by applying the simulation parameters given by Equation (30), geometric phases can be obtained.

4.2. Elimination of the Dynamical Phase in Spin-Magnetic Field Photonic Simulation

It is well known in the mechanical case that the geometric phase is hidden in the spin-magnetic field interaction because it is combined with the dynamical phase within ϕ^\pm ; therefore, the dynamical phase has to be eliminated in order to take advantage of the properties of a geometric phase. We present a photonic solution, which is similar to the one used in the mechanical case, that is if the quantum state, after evolution under a first Hamiltonian $\hat{H}_1 = \hat{H}$ for time T , finds a second Hamiltonian $\hat{H}_2 = -\hat{H}$, then the dynamical phase are mutually canceled; however, the eigenstates do not change, therefore neither does the geometrical phase.

In the photonic case, we have to find a new momentum operator, that is a new integrated optical grating, such as $\hat{M}_2 = -\hat{M}$. We assume that such a new optical grating has the same frequency γ ; therefore, we have the same rotating system, that is the same transformation (28). Accordingly, the condition for eliminating the dynamical phase is obtained from the operator \hat{M}' , that is,

$$\hat{M}'_2 = \frac{\hbar}{2} \begin{pmatrix} \Delta\beta' - \gamma & C'_o \\ C'_o & -\Delta\beta' + \gamma \end{pmatrix} = -\hat{M}' = -\frac{\hbar}{2} \begin{pmatrix} \Delta\beta - \gamma & C_o \\ C_o & -\Delta\beta + \gamma \end{pmatrix}; \quad (48)$$

therefore, $C'_o = -C_o$ and $(\Delta\beta - \gamma) = -(\Delta\beta' - \gamma)$. The first condition can be achieved by introducing an initial phase in the second grating, that is $\Delta\epsilon(x, z) = \Delta\epsilon(x) \cos(\gamma z + \pi)$, and the second one is achieved if $\Delta\beta' = 2\gamma - \Delta\beta$. These results indicate that we need an additional grating with a new difference between propagation constants (linear momentum of the photon) $\Delta\beta' = (\beta'_0 - \beta'_1)$. In Figure 5 the system for eliminating the dynamical phase is shown. Therefore, the total phases are $\phi_\pm = \nu(\mp p\Lambda/\hbar - \pi)$, and the dynamical phases are:

$$\phi_d^\pm = \frac{p_\pm}{\hbar} \nu\Lambda \mp \nu\pi \cos \alpha' \quad (49)$$

Therefore, the total dynamical phase is $\Phi_d = 0$, and the total geometrical phase after the single-photon state propagates through the two integrated gratings is twice the value acquired in the first grating, that is,

$$\Phi_g^\pm = \mp 2\nu\pi(1 - \cos \alpha') = \mp \Phi_g. \quad (50)$$

Alternatively, propagation constants can be unchanged, and the grating frequency can be modified, that is $\gamma' = 2\Delta\beta - \gamma$; however, in this case, the transformation (28) must be applied with the factor γ' . In short, we eliminated the dynamical phase; therefore, these results could be used for implementing logic gates or transformations based on topological phases, which are much more insensitive to fabrication errors, unlike dynamical phases, which as mentioned are of order ω . With these results, robust P-gates (Phase gates) can be designed; thus, the following transformation is implemented between the eigenstates:

$$P = \begin{pmatrix} \exp(-i2\nu\pi \cos \alpha') & 0 \\ 0 & \exp(i2\nu\pi \cos \alpha') \end{pmatrix} = \exp(-i\Phi_g \sigma_z) \quad (51)$$

Note that for $4\nu \cos \alpha' = \pm 1$, a Z-gate is obtained, and for $4\nu \cos \alpha' = \pm 1/2$, an S-gate is implemented, and so on.

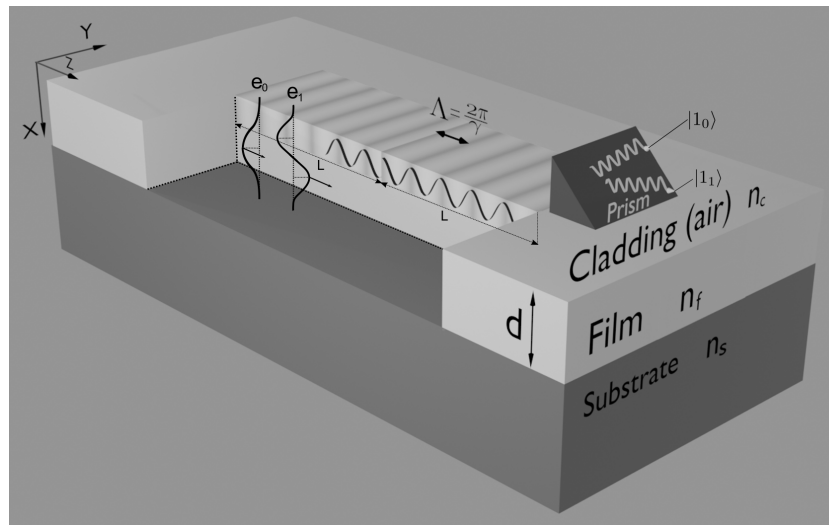


Figure 5. Elimination of the dynamical phase by using two consecutive integrated optical gratings. The second grating has an initial phase π . Likewise, a prism is used to make a projective measure of states $|1_0\rangle$ and $|1_1\rangle$ for obtaining the probabilities P_0 and P_1 and, therefore, the geometric phase Φ_g .

4.3. Geometric Phases with Other Quantum States

On the other hand, the eigenstates given by Equation (31) can be written as single-photon states excited in rotated optical modes, that is $e_+(x, y) = \cos \frac{\alpha'}{2} e_0(x, y) + \sin \frac{\alpha'}{2} e_1(x, y)$ and $e_-(x, y) = -\sin \frac{\alpha'}{2} e_0(x, y) + \cos \frac{\alpha'}{2} e_1(x, y)$; therefore:

$$|l_+(0)\rangle = \cos \frac{\alpha'}{2} |1_0\rangle + \sin \frac{\alpha'}{2} |1_1\rangle = |1_+\rangle, \quad |l_-(0)\rangle = -\sin \frac{\alpha'}{2} |1_0\rangle + \cos \frac{\alpha'}{2} |1_1\rangle = |1_-\rangle \quad (52)$$

The elimination of the dynamical phase means that these eigenstates have undergone the transformation $e^{\pm i\Phi_g} |1_{\pm}\rangle$; therefore, the following formal relationships can be written:

$$e^{i\Phi_g} |1_+\rangle = e^{i\Phi_g} \hat{a}_+^\dagger |0_{\pm}\rangle, \quad e^{-i\Phi_g} |1_-\rangle = e^{-i\Phi_g} \hat{a}_-^\dagger |0_{\pm}\rangle \quad (53)$$

with $\Phi_g = -2v\pi(1 - \cos \alpha')$. Accordingly, the following transformations, induced by geometric phases, for the absorption operators are obtained:

$$\hat{a}_{\pm}(z = n\Lambda) = e^{\pm i\Phi_g} \hat{a}_{\pm}(0) \quad (54)$$

This result can be used for obtaining geometric phases of other quantum light states. As an example, we present two states, that is the number photon state or Fock state $|n_+\rangle$ and the coherent state $|\alpha_+\rangle$, where subindex + indicates that the state is excited in the optical mode $e_+(x, y)$. The Fock state under propagation becomes:

$$|n_+(0)\rangle = \frac{1}{\sqrt{n_+!}} (\hat{a}_+(0)^\dagger)^{n_+} |0\rangle \longrightarrow \frac{1}{\sqrt{n_+!}} e^{in_+\Phi_g} (\hat{a}_+^\dagger)^{n_+} |0\rangle = e^{in_+\Phi_g} |n_+\rangle \quad (55)$$

Therefore, the quantum state has acquired a geometric phase $n_+\Phi_g$. Likewise, the coherent state can be rewritten by using the complex displacement operator, that is,

$$|\alpha_+(0)\rangle = e^{(\alpha_+ \hat{a}_+^\dagger(0) - c.h.)} |0\rangle \longrightarrow e^{(\alpha_+ e^{i\Phi_g} \hat{a}_+^\dagger - c.h.)} |0\rangle = |e^{i\Phi_g} \alpha_+\rangle \quad (56)$$

Therefore, the geometric phase is Φ_g , that is the same as the one acquired by a single photon. The same procedure can be applied to any other quantum light state excited in the integrated photonic grating.

4.4. Optical Measurement of Geometric Phases

Finally, we present how to measure the geometric phase starting from the measurements of the single-photon detection probability, which can be extracted by a prism-waveguide coupler [10], as shown in Figure 5. We focus on the spin-magnetic field interaction simulation case. By assuming that the input state is a single photon excited in the mode $e_0(x, y)$ and taking into account the relationships given by Equation (52), the following final state is obtained after the two gratings:

$$|L(z)\rangle = (\cos^2 \frac{\alpha'}{2} + \sin^2 \frac{\alpha'}{2} e^{i\Phi_g})|1_0\rangle + \cos \frac{\alpha'}{2} \sin \frac{\alpha'}{2} (1 - e^{i\Phi_g})|1_1\rangle \quad (57)$$

The probability of the detection of a photon in Mode 0, that is P_0 , or in Mode 1, P_1 , is a function of the geometric phase, that is,

$$P_1 = \frac{\sin^2 \alpha}{2} (1 - \cos \Phi_g), \quad P_0 = 1 - P_1 \quad (58)$$

If $\Phi_g = 2\pi$, then $P_1 = 0$ and $P_0 = 1$, and if $\Phi_g = \pi$, then $P_1 = \sin^2 \alpha$ and $P_0 = \cos^2 \alpha$. Therefore, from the measurement of P_1 and P_0 , the phase Φ_g is obtained. In Figure 5 it is shown the projective measure of states $|1_0\rangle$ and $|1_1\rangle$ by a prism-waveguide coupler, which projects these state in different spatial directions. Finally, note that by using a coherent state, these probabilities are proportional to the intensity of the light, what can be called a semiclassical optical characterization, or in the most technical way, the geometric phase is also acquired by the classical fields, but would rigorously correspond to the so-called Hannay phase [33].

4.5. Geometric Phases in Light-Matter Photonic Simulation

Finally, we check that light-matter simulation can be also used to obtain geometric phases. For the sake of simplicity, we show geometric phases for wedge circuits, although more general cases can be studied. Let us consider an initial state $|L(0)\rangle = |1_0\rangle$, that is the point $(0, 0, 1)$ on the photonic Bloch sphere. Next, let us consider an asynchronous optical grating with $\delta_s \ll C_o$; therefore, according to Equation (37) (phase gate), for $\delta_s z_0 = 3\pi/2$, we obtain $|L(z_0)\rangle = (1/\sqrt{2})(|1_0\rangle + i|1_1\rangle)$, that is the state reaches the Bloch sphere point $(0, 1, 0)$. Next, we consider that the grating has a greater coupling coefficient C_o , then the single-photon state is given by the expression:

$$|L(z)\rangle = \frac{1}{\sqrt{2}} [(\cos \frac{\delta_r z}{2} + b \sin \frac{\delta_r z}{2} + ia \sin \frac{\delta_r z}{2})|1_0\rangle + (a \sin \frac{\delta_r z}{2} + i \cos \frac{\delta_r z}{2} - ib \sin \frac{\delta_r z}{2})|1_1\rangle] \quad (59)$$

where $a = \delta_s/\delta_r$ and $b = C_o/\delta_r$. If we choose a distance $z = z_1$ such as $\delta_r z_1/2 = \pi/2$, then, after a certain calculation, the following state is obtained:

$$|L(z_1)\rangle = \frac{e^{i\phi_o}}{\sqrt{2}} (|1_0\rangle + i|1_1\rangle) \quad (60)$$

where $\phi_o = \text{atan}(a/b) = \text{atan}(\delta_s/C_o)$, that is $a = \sin \phi_o$ and $b = \cos \phi_o$. The state has reached the point $(0, -1, 0)$ of the photonic Bloch sphere. Now, we show that ϕ_o is a geometric phase. Indeed, for the sake of symmetry, the state before reaching the above state has crossed the meridian $y = 0$ when $\delta_r z/2 = \pi/4$, that is, the state:

$$|L'\rangle = \frac{(1 + b + ia)}{2} |1_0\rangle + \frac{(a + i(1 - b))}{2} |1_1\rangle \equiv m_0 e^{i\epsilon_0} |1_0\rangle + m_1 e^{i\epsilon_1} |1_1\rangle. \quad (61)$$

It is easy to prove that both states have the same phase, that is $\epsilon_0 = \epsilon_1$, and the modulus is given by $m_0 = \sin(\phi_o/2)$ and $m_1 = \cos(\phi_o/2)$; therefore, the state crosses the point $P = (\sin \phi_o, 0, \cos \phi_o)$ of the photonic Bloch sphere as indicated in Figure 4 for $\varphi = \phi_o$. Now, we must recall that partial

cycles also generate geometric phases, which can be calculated by closing the end points of the open cycle by a geodesic line [28,30]. In our case, the corresponding geodesic lies along the meridian at the plane $x = 0$, from point $(0, -1, 0)$ to initial point $(0, 0, 1)$. In short, the state has followed a wedge circuit C_w , as shown in Figure 4. Now, we calculate the subtended solid angle by this wedge circuit. It is easy to check that a wedge circuit with angle ϕ_o subtends a solid angle $\Omega(C_w) = 2\phi_o$; therefore, the geometric phase is $\Phi_g = (1/2)\Omega(C_w) = \phi_o = \text{atn}(\delta_s/C_o)$, which is just the global phase obtained in Equation (60). It is worth underlining that in this case, the geometric phase is not hidden, and therefore, the dynamical phase does not have to be eliminated. Moreover, this geometric phase can be also obtained in a atom-optical field system out of resonance by using Θ -pulses, with the first optical field with low amplitude E_o (Z gate) and the next with a higher amplitude E_o . By using the simulation parameters given by Equation (34), the geometric phase would be $\Phi_g = \text{atn}(\delta/\Omega)$.

5. Conclusions

We propose a quantum photonic device based on integrated optical gratings in a two-mode slab guide to simulate the interaction between external fields and atoms. By using single-photon states, we study the simulations of a spin-(1/2)-magnetic field system, as for example nuclear magnetic resonance, and a two-level atom-optical field system corresponding to light-matter simulation. Both dynamical and geometric properties are simulated, in particular the geometric phases obtained by the mentioned systems. We prove that dynamical properties can be simulated for a wide range of cases with practical interest, although in the spin-(1/2)-magnetic field system it is restricted to relatively high values of frequency and magnetic field amplitude B_o . Overall, atom-optical field interaction does not present these restrictions. This study of integrated optical gratings opens up possibilities to more general simulations if several modes are used. Thus, spin (s)-magnetic field interaction simulations could be implemented by using a number $N = 2s+1$ of codirectional optical modes assisted by optical gratings; multilevel atom (n)-optical field interaction can be simulated by using $N = n$ collinear optical modes coupled by optical gratings, which can in turn simulate, for example, two-qubit single photon logic gates, which has a high interest in quantum information systems; likewise, optical gratings allow interaction between d collinear modes, and thus, simulators based on N codirectional modes can reduce the number of paths used up to N/d , which improves the optical integration of the photonic simulator. On the other hand, AA geometric phases have been also obtained for both systems. The spin-(1/2)-magnetic field system requires dynamic phase cancellation, which is simulated by using two optical gratings; however, in the atom-optical field system, such cancellation is not required. Obviously, we must emphasize that although the proposed integrated photonic device is intended for quantum simulation, it can also be used to implement quantum operations and/or effects with the photonic device itself, such as logic gates, geometric phases, and so on, by using single-photon states or more general quantum states, as shown.

Author Contributions: All authors contributed equally to this work. All authors read and agreed to the published version of the manuscript.

Funding: Xunta de Galicia, Consellería de Educación, Universidades e FP, Grant GRC Number ED431C2018/11; Ministerio de Economía, Industria y Competitividad, Gobierno de España, Grant Number AYA2016-78773-C2-2-P.

Acknowledgments: One of the authors (G.M.C.) wishes to acknowledge the financial support by Xunta de Galicia, Consellería de Educación, Universidades e FP, by a predoctoral grant co-financed with the European Social Fund.

Conflicts of Interest: The authors declare no conflict of interest. The funders had no role in the design of the study; in the collection, analyses, or interpretation of data; in the writing of the manuscript; nor in the decision to publish the results.

Abbreviations

The following abbreviations are used in this manuscript:

RWA	Rotating Wave Approximation
NMR	Nuclear Magnetic Resonance
AA	Aharonov–Anandan
SPDC	Spontaneous Parametric Down Conversion
DC	Directional Coupler
SDC	Selective Directional Coupler
APD	Avalanche Photodiode
SMW	Single-Mode Waveguide
TMW	Two-Mode Waveguide
OG	Optical Grating

References

- Huttner, B.; Serulnik, S.; Ben-Aryeh, Y. Quantum analysis of light propagation in a parametric amplifier. *Phys. Rev. A* **1990**, *42*, 5594–5600. [[CrossRef](#)]
- Liñares, J.; Nistal, M. Quantization of coupled modes propagation in integrated optical waveguides. *J. Mod. Opt.* **2003**, *50*, 781–790. [[CrossRef](#)]
- Johnson, T.H.; Clark, S.R.; Jarsch, D. What is a quantum simulator? *EPJ Quantum Technol.* **2014**, *1*, 10. [[CrossRef](#)]
- Georgescu, I.; Ashhab, S.; Nori, F. Quantum simulation. *Rev. Mod. Phys.* **2014**, *86*, 153–185. [[CrossRef](#)]
- Schaetz, T.; Monroe, C.R.; Esslinger, T. Focus on quantum simulation. *New J. Phys.* **2013**, *15*, 085009. [[CrossRef](#)]
- Agarwal, G. *Quantum Optics*; Cambridge University Press: Cambridge, UK, 2013.
- Longui, S.; Della Valle, G. Anyons in one-dimensional lattices: A photonic realization. *Opt. Lett.* **2012**, *37*, 2160–2162. [[CrossRef](#)]
- Le Bellac, M. *A Short Introduction to Quantum Information and Quantum Computation*; Cambridge University Press: Cambridge, UK, 2006.
- Loudon, R. *The Quantum Theory of Light*; Oxford University Press: Oxford, UK, 2003.
- Lee, D. *Electromagnetic Principles of Integrated Optics*; Wiley: New York, NY, USA, 1986.
- Doerr, C. Silicon photonic integration in telecommunications. *Front. Phys.* **2015**, *3*, 7–22. [[CrossRef](#)]
- Politi, A.; Matthews, J.C.F.; Thompson, M.G.; O’Brien, J.L. Integrated Quantum Photonics. *IEEE J. Sel. Top. Quantum Electron.* **2009**, *15*, 1673–1684. [[CrossRef](#)]
- Wang, J.; Sciarrin, F.; Laing, A.; Thompson, M. Integrated photonic quantum technologies. *Nat. Photonics* **2020**, *14*, 273–284. [[CrossRef](#)]
- Company, J.; Pérez, D. *Programmable Integrated Photonics*; Oxford University Press: Oxford, UK, 2020.
- Liñares, J.; Montero, C.; Moreno, V.; Nistal, M.C.; Prieto, X.; Salgueiro, J.R.; Sotelo, D. Glass processing by ion exchange to fabricate integrated optical planar components: Applications. *Proc. SPIE* **2000**, *3936*, 227–238.
- Righini, G.; Chiappini, A. Glass optical waveguides: A review of fabrication techniques. *Opt. Eng.* **2014**, *53*, 071819. [[CrossRef](#)]
- Cacciari, I.; Brenci, M.; Falciai, R.; Conti, G.; Pelli, S.; Righini, G. Reproducibility of splicer-based long-period fiber gratings for gain equalization. *Front. Phys.* **2007**, *3*, 203–206. [[CrossRef](#)]
- Yao, Y.; Liu, H.; Xue, L.; Liu, B.; Zhang, H. Design of lithium niobate phase-shifted Bragg grating for electro-optically tunable ultra-narrowbandwidth filtering. *Appl. Opt.* **2019**, *58*, 6770–6774. [[CrossRef](#)] [[PubMed](#)]
- Ben-Aryeh, Y.; Serulnik, S. The quantum treatment of propagation in non-linear optical media by the use of temporal modes. *Phys. Lett. A* **1991**, *155*, 473–479. [[CrossRef](#)]
- Liñares, J.; Nistal, M.; Barral, D. Quantization of Coupled 1d Vector Modes In Integrated Photonics Waveguides. *New J. Phys.* **2008**, *10*, 063023. [[CrossRef](#)]
- Liñares, J.; Nistal, M.; Barral, D.; Moreno, V. Optical field-strength polarization of two-mode single-photon states. *Eur. J. Phys.* **2010**, *31*, 991–1005. [[CrossRef](#)]
- Fox, M. *Quantum Optics*; Oxford University Press: Oxford, UK, 2006.

23. Englert, B.; Kurtsiefer, C.; Weinfurter, H. Universal unitary gate for single-photon two-qubit states. *Phys. Rev. A* **2001**, *63*, 032302. [[CrossRef](#)]
24. Spring, J.; Metcalf, B.; Humphreys, P.; Kolthammer, W.; Jin, X.; Barbieri, M.; Datta, A.; Thomas-Peter, N.; Langford, N.K.; Kundys, D.; et al. Boson sampling on photonic chip. *Science* **2013**, *239*, 798–801. [[CrossRef](#)]
25. de Guise, H.; Di Matteo, O.; Sánchez-Soto, L. Simple factorization of unitary transformations. *Phys. Rev. A* **2018**, *97*, 022328. [[CrossRef](#)]
26. Berry, R. Quantal phase factors accompanying adiabatic change. *Proc. R. Soc. Lond. A* **1987**, *392*, 45–64.
27. Aharonov, Y.; Anandan, J. Phase change during a cyclic quantum evolution. *Phys. Rev. Lett.* **1987**, *58*, 1593–1596. [[CrossRef](#)]
28. Jordan, T. Berry phases for partial cycles. *Phys. Rep.* **1988**, *38*, 1590–1592. [[CrossRef](#)]
29. Bhandari, R. Polarization of light and topological phases. *Phys. Rep.* **1997**, *281*, 1–64. [[CrossRef](#)]
30. Liñares, J.; Nistal, M. Geometric phases in multidirectional electromagnetic coupling theory. *Phys. Lett. A* **1992**, *162*, 7–14. [[CrossRef](#)]
31. Ekert, A.; Ericsson, M.; Hayden, P.; Inamori, H.; Jones, J.; Oi, D.; Vedral, V. Geometric quantum computation. *J. Mod. Opt.* **2000**, *47*, 2501–2513. [[CrossRef](#)]
32. Sjöqvist, E. Geometric phases in quantum information. *Int. J. Quantum Chem.* **2015**, *115*, 1311–1326. [[CrossRef](#)]
33. Agarwal, T.; Simon, R. Berry phase, interference of light beams and the Hannay angle. *Phys. Rev. A* **1990**, *42*, 6924–6927. [[CrossRef](#)]

Publisher’s Note: MDPI stays neutral with regard to jurisdictional claims in published maps and institutional affiliations.



© 2020 by the authors. Licensee MDPI, Basel, Switzerland. This article is an open access article distributed under the terms and conditions of the Creative Commons Attribution (CC BY) license (<http://creativecommons.org/licenses/by/4.0/>).